iScience

CellPress
OPEN ACCESS

Article

Interference of electrochemical ion diffusion in nanopore sensing

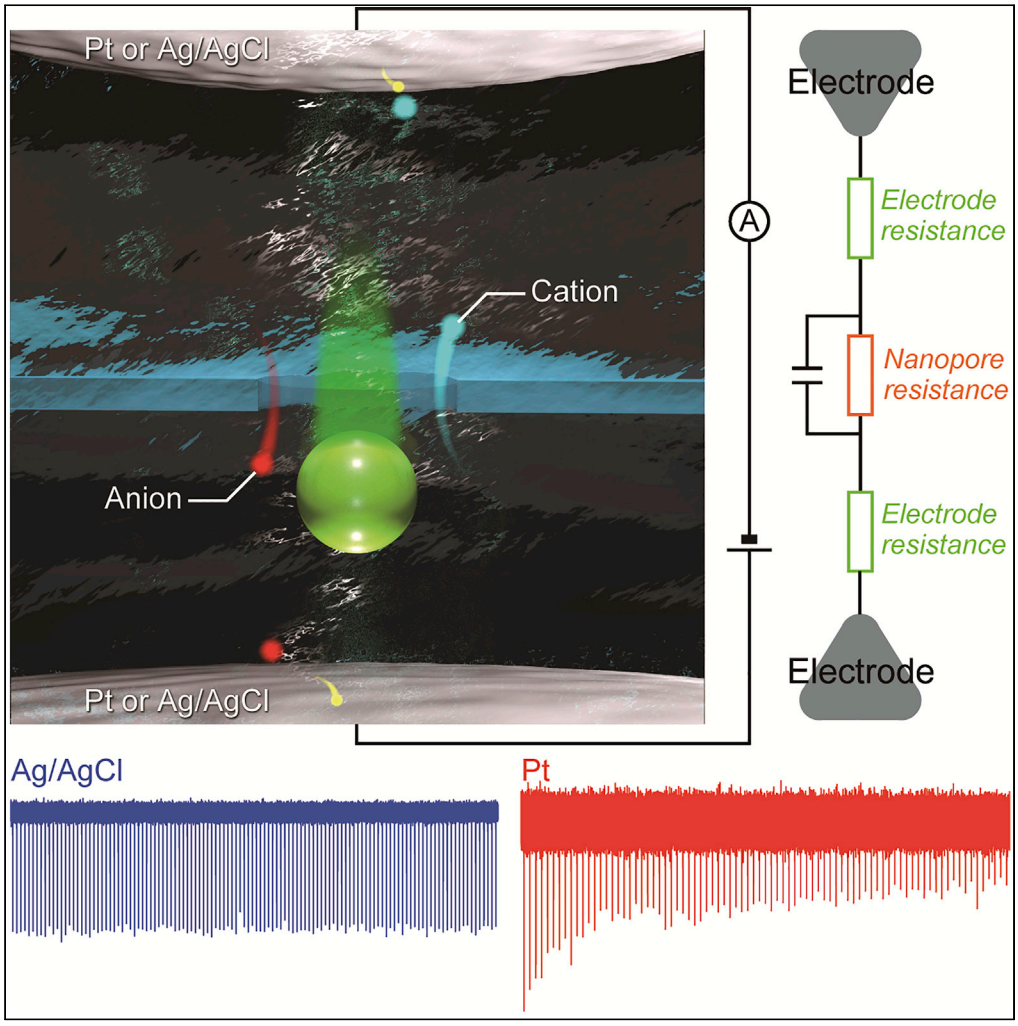

Iat Wai Leong, Shohei Kishimoto, Makusu Tsutsui, Masateru Taniguchi

makusu32@sanken.osaka-u.ac.jp

Highlights

Ag/AgCl electrodes enable reliable resistive pulse detections of nanoparticles

Pt electrodes induce ionic current decay by time via the Cottrell diffusion

Cottrell diffusion deteriorates the nanopore sensor temporal resolution

Leong et al., iScience *25*, 105073
October 21, 2022
https://doi.org/10.1016/j.isci.2022.105073

iScience

CellPress
OPEN ACCESS

Article

Interference of electrochemical ion diffusion in nanopore sensing

Iat Wai Leong,[1,2] Shohei Kishimoto,[1,2] Makusu Tsutsui,[1,3,*] and Masateru Taniguchi[1]

SUMMARY

Stable and fast-responding ionic current is a prerequisite for reliable measurements of small objects with a nanopore. Here, we report on the interference of ion diffusion kinetics at liquid-electrode interfaces in nanopore sensing. Using platinum as electrodes, we observed a slow and large decrease in the ionic current through a nanopore in a salt solution suggestive of the considerable influence of the growing impedance at the liquid-metal interfaces via Cottrell diffusion. When detecting nanoparticles, the resistive pulses became weaker following the steady increase in the resistance at the partially polarizable electrodes. The interfacial impedance was also demonstrated to couple with the nanopore chip capacitance thereby degraded the temporal resolution of the ionic current measurements in a time-varying manner. These findings can be useful for choosing the suitable size and material of electrodes for the single-particle and -molecule analyses by ionic current.

INTRODUCTION

Nanopore is a powerful tool for analyzing biological samples at a single-molecule level (Xue et al., 2020; Hu et al., 2020; He et al., 2021; Fried et al., 2021). It is a conductometer that detects a temporal change of the ion flow in a nanoscale conduit upon translocation of an object via ionic current measurements (Henriquez et al., 2004), the simple mechanism of which has been demonstrated to enable a versatile sensor for identifying miscellaneous analytes from cells to genomes (Xue et al., 2020; Hu et al., 2020; He et al., 2021; Fried et al., 2021; Henriquez et al., 2004; Sun and Morgan, 2010). Being electrochemical in nature, meanwhile, the electrical current generally reflects the dynamic phenomena at the electrode-liquid interfaces (Zhang et al., 2006; Gao et al., 2019). Specifically, the application of voltage perturbs the local ion distribution by overconsuming reactants for the electrochemical reactions, which induces subsequent ion motions in the bulk to relax the acute ion concentration gradient near the electrode surface (Pletcher et al., 2011). This Cottrell diffusion causes a gradual decrease in the ionic current over time, whose characteristics provide rich information concerning the properties of ions in chronoamperometry (Messerschmitt et al., 2014; Lee et al., 2018). However, little effort has been devoted to investigate its relevance to the nanopore sensing (Zhang et al., 2006), where the time-course change in the impedance outside the pore may cause critical effects on the temporal resolution of the ionic current measurements for detecting small molecules and particles (Plesa et al., 2013, 2015; Tsutsui et al., 2021). In the present study, therefore, we explored this issue by comparing resistive pulse measurements of nanoparticles using multiple kinds of electrodes (Figure 1).

RESULTS

Resistive pulse measurements using Ag/AgCl electrodes

A nanopore of diameter 300 nm in a 40-nm thick SiN_x membrane was used to detect 178-nm-sized polymeric beads in phosphate buffered saline at a concentration of 10^9 particles/mL (zeta potential of −37 to −30 mV in the electrolyte buffer of pH 7.6 containing 55 to 137 mM NaCl as measured by a zeta sizer) by recording the ionic current I_{ion} under the applied voltage V_b (V_b is 0.4 V unless otherwise noted). We start with a case of Ag/AgCl, which is a typical compound used in nanopore measurements (Wang et al., 2022; Mojtabavi et al., 2022). It provided a persistent current flow with slow ups and downs (Figure 2A) associated with concentration fluctuations of reactants and products via their adsorption and precipitation at the surface under the electrochemical reactions in chloride solutions (Pletcher et al., 2011). In the meantime, resistive pulses were observed as the polymer nanoparticles passed through the pore by electrophoresis. These

[1]The Institute of Scientific and Industrial Research, Osaka University, Mihogaoka 8-1, Ibaraki, Osaka 567-0047, Japan

[2]These authors contributed equally

[3]Lead contact

*Correspondence: makusu32@sanken.osaka-u.ac.jp

https://doi.org/10.1016/j.isci.2022.105073

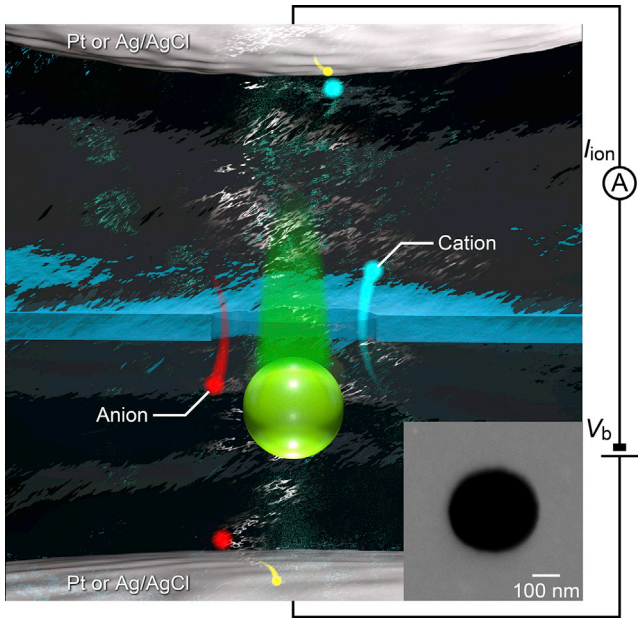

Figure 1. Schematic model depicting nanopore sensing of single-nanoparticles

The ionic current I_{ion} flowing through a nanopore in a SiN_x membrane is measured in a phosphate buffered saline containing various concentrations of NaCl under the applied voltage V_b. Transient drops in I_{ion} upon electrophoretic translocation of the negatively charged polymeric nanobeads were recorded using two different electrodes, Ag/AgCl and Pt. Inset is a scanning electron micrograph of a 300 nm diameter pore in a 40 nm thick SiN_x membrane used for the resistive pulse measurements.

signals showed little variations in their heights (Figure 2B) representative of the narrow size distributions of the synthetic nanobeads (varying by less than 11% from the average particle diameter of 178 nm as confirmed by a dynamic light scattering method). There are also no notable changes in the pulse-like waveforms with time for the entire range of the salt concentration conditions tested, which suggested minor influence of the ion diffusion at the solution-electrode interfaces on the resistive pulse sensing.

To verify the accuracy of the single-particle measurements, we theoretically estimated the ionic blockade current by the polymeric sphere (Figure S1) (Tsutsui et al., 2019; Liao et al., 2020). Finite element calculations based on coupled Poisson-Nernst Planck and Navier Stokes equations predicted a drop in I_{ion} (ΔI_{ion}) by approximately 15 nA when a 170-nm-sized particle was moved along the pore axis under the salt concentration of 123 mM NaCl (Figure 2C). The experimental ΔI_{ion} - t traces revealed similar features except the asymmetric signal line-shapes demonstrating the relatively slow motions at the nanopore orifice due to the hydrodynamic dragging under the electroosmotic flow (water flows in a direction opposite to the electrophoresis of the negatively charged particles in the SiN_x nanopore for its negative native charge on the wall surface) (van Dorp et al., 2009; Firnkes et al., 2010). Moreover, the simulations indicated a linear rise in the resistive pulse height I_p with the open pore current I_{open} (Figure 2D), which is in fair agreement with the experimental observations (Figure 2E). It can be interpreted by the fact that the electrolyte concentrations affect the homogeneous resistivity of the solution ($1/\rho$) including the open volume in the partially occluded nanopore by the particle. This in turn provides a transmission line circuit model of the fluidic system as a simple resistor of the resistance $R_{pore} = \rho(4L/\pi d_{pore}^2 + 1/d_{pore})$ at the nanopore (Garaj et al., 2010; Kowalczyk et al., 2011) with negligible contributions of the electrodes (apart from the slight change in I_p in response to the time-course decrease in I_{open} by less than 10% ascribable to the small yet finite effects of the resistance at the electrolyte solution-Ag/AgCl interfaces (Figure S2)).

Cottrell diffusion observed in Pt/nanopore/Pt systems

Measuring the polymeric beads using the same nanopore but with platinum electrodes instead of Ag/AgCl, we found quite different ionic current characteristics showing a large decrease in I_{open} over time (Figure 3A). Furthermore, while the nanoparticles still could be detected, the resistive pulses became steadily weaker along the diminishing open pore current (Figures 3B–3E). Here, what is different in platinum from

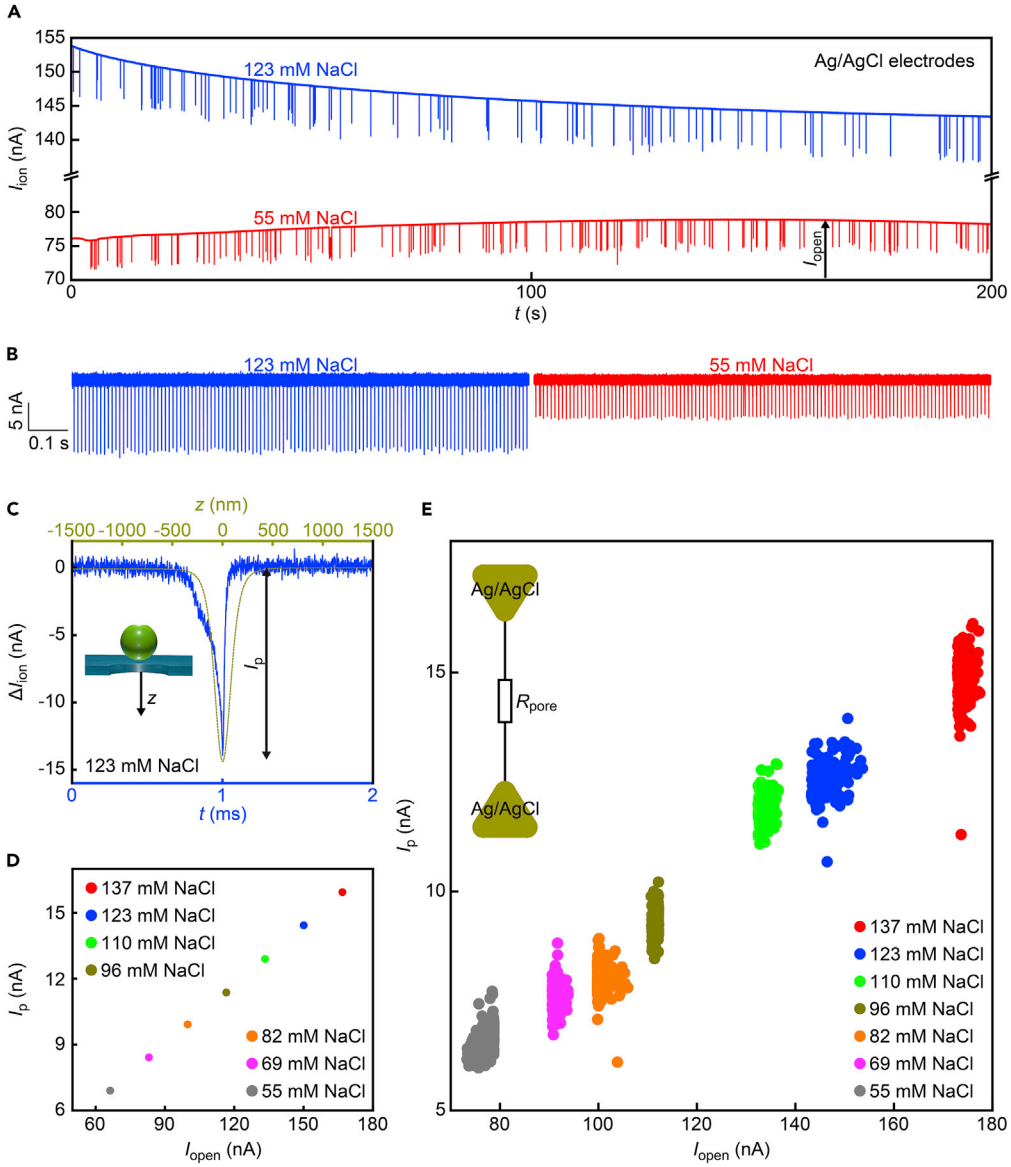

Figure 2. Open pore and blockade current characteristics observed with Ag/AgCl electrodes

(A) Partial ionic current traces recorded in a dilute suspension of 186 nm-sized polymeric nanobeads in phosphate buffered saline containing 123 mM (blue) and 55 mM (red) NaCl using a 300 nm-sized SiN_x nanopore with Ag/AgCl electrodes under the transmembrane voltage V_b of 0.4 V.

(B) Resistive pulses of equal heights detected in the 123 mM (blue) and 55 mM (red) NaCl solutions. The open pore current is offset to zero.

(C) A magnified view of a resistive pulse in 123 mM NaCl (blue) compared with a simulated ionic signal for a 170 nm particle passing through a 300 nm diameter channel (dark yellow). The open pore current is offset to zero. z denotes the position of the particle center.

(D) The resistive pulse height I_p versus the open pore current I_{open} obtained by the finite element simulations of the particle translocation in aqueous solutions of various NaCl concentrations.

(E) Experimental I_p under various salt concentration conditions plotted as a function of the open pore current I_{open} at the moment when the resistive pulses were detected. Inset is an equivalent circuit model of the nanopore. There is no additional impedance at the solution/electrode interfaces due to the electrochemical nature of Ag/AgCl in the chloride solution.

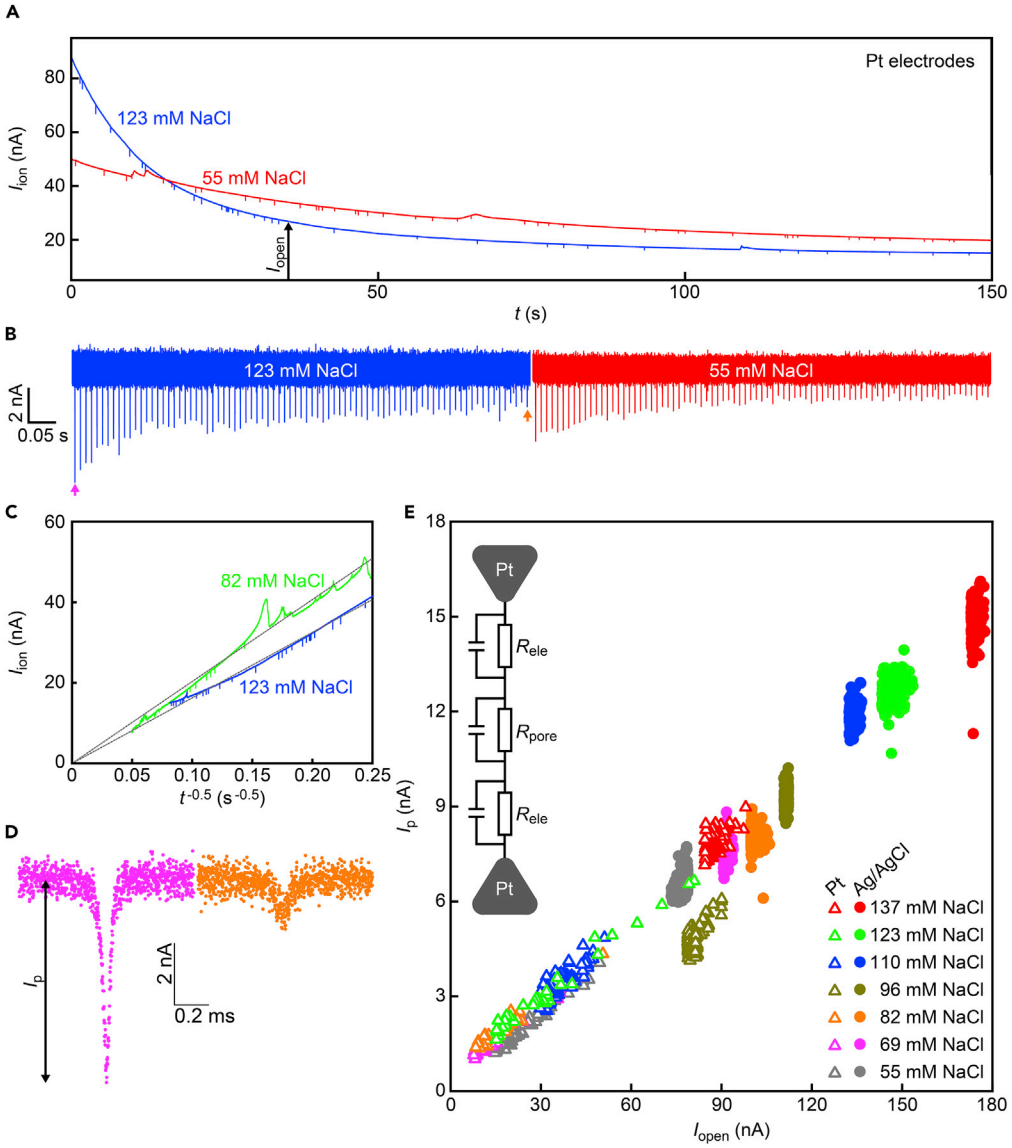

Figure 3. Time-varying Faraday current and resistive pulses in a Pt-nanopore-Pt setup

(A) Partial I_{ion} traces in 123 (blue) and 55 mM (red) NaCl solutions recorded using a 300 nm-sized nanopore with Pt electrodes under V_b of 0.4 V. Large spike-like features are presumably due to charging/discharging.

(B) Resistive pulses of varying heights observed in 123 (blue) and 55 mM (red) NaCl.

(C) The ionic current curves displayed as a function of $t^{-0.5}$. Gray lines are linear fitting to the data.

(D) Resistive pulses observed at the beginning (pink arrow in (b)) and the end (orange arrow in (b)) of one measurement.

(E) The measured I_p with Pt (open triangles) and Ag/AgCl (filled circles) plotted with respect to I_{open} at the moment when the resistive pulses appeared. Inset is a circuit model of the Pt-nanopore-Pt system with impedance at the solution/electrode interfaces serially connected to the resistance at the pore.

Ag/AgCl is the electrochemical reactions in the chloride solution involving no precipitation/adsorption of the reactants. In such a case, the Faraday current is expected to diminish monotonically rather than stay stable at a certain level, as the non-equilibrium ion concentration gradients at the voltage-biased electrode surface tend to be flattened by time via the diffusive motions of ions in the bulk solution (Plesa et al., 2015). In the case of parallel plate electrodes without a nanopore membrane, Fick's law describes the time-dependent Faraday current to behave as $I_{ion} = nFAD^{0.5}c/(\pi t)^{0.5}$, where F is the Faraday constant, A is the water-touching electrode area, D and c are the diffusion constant and the concentration of ions, and n is the number of electrons worked in the electrochemical reaction (Plesa et al., 2015). Indeed, the deep I_{open}

drop was found to occur as $t^{-0.5}$ (Figure 3C) thereby manifested that the transmembrane ionic current is limited by the ion diffusion at the electrodes. More quantitatively, tentatively assuming water dissociation reactions on Pt surfaces in the pH7.6 buffer (van der Niet et al., 2013; Jaksic et al., 1993), we obtain D of 7.0×10^{-8} m^2/s from the $t^{-0.5}$ fitting (solid line in Figure 3C) with the electrode area of 2.7×10^{-5} m^2. While this value is close to the diffusion constants of H^+ and OH^- at ambient conditions (Lee and Rasaiah, 2011; Holz et al., 2000), it should also be pointed out that V_b is lower than the voltage required for initiating Faraday electrolysis of water. Further efforts should thus be devoted to shed light on the electrochemical reactions responsible for the nanopore ionic current in the Pt/nanopore/Pt system.

Electrode material and electrolyte dependence of Cottrell behaviors

Extending the experiments to different electrode materials (Figure 4A), we obtained stable ionic current as well as uniform height resistive pulses of the polystyrene nanoparticles with Ti (Figure 4B). This demonstrates that Ti is equally useful to Ag/AgCl for nanopore sensing owing presumably to its dissolution reactions under the electric potential difference (Baehre et al., 2016). In case of Ag, the open pore current as well as the resistive pulse heights tended to become lower over time. It is naturally ascribed to the absence of AgCl for the precipitation/adsorption-mediated electrochemical reactions that led the Cottrell diffusion to become observable in the ionic current traces. Au also displayed similar behavior due to its electrochemically inert properties.

Moreover, we tested salts other than NaCl. In case of a mixture aqueous solution of $K_3Fe(CN)_6$ and $K_4Fe(CN)_6$ (Figure 4C), the redox reactions involving precipitations (Luo et al., 2017), similar to those occurring at the Ag/AgCl electrodes in chloride solutions, provided stable ionic current even with Pt electrodes though not applicable for the resistive pulse detections (Figure 4D) perhaps due to the aggregation of the polystyrene nanobeads via the electrostatic interactions with the multivalent ions in the solution. On the other hand, a Cottrell behavior was observed when replacing the solution with the one containing only $K_3Fe(CN)_6$ since the redox reactions cannot take place without $K_4Fe(CN)_6$. These results were consistent to validate the pronounced roles of the electrochemical ion diffusion on the nanopore sensing.

Roles of electrode material on nanopore sensor temporal resolution

How about its impact on the nanopore sensing? The resistive pulses were already explained to become smaller over time (Figure 3D). To be more quantitative, we plotted the signal heights with respect to the open pore current. They revealed a proportionality between I_p and I_{open} even for the data in a single measurement under a specific salt concentration condition (Figure 3E), which implies a direct relevance of the impedance at the solution/platinum interfaces on the ionic blockade current. Interestingly, the Ag/AgCl results were also in line with the linear dependence. Nevertheless, it should be noted that the underlying mechanisms are completely different. In the Ag/AgCl measurements, we changed the resistivity of the whole nanopore system by the salt concentration conditions that affected I_p and I_{open} on the same footing (Henriquez et al., 2004). On the other hand, the ion diffusion at the voltage-biased platinum yielded local impedance at the liquid-electrode interfaces. In this sense, I_p is expected to scale with I_{open}^2 when assuming a serially connected resistor of resistance R_{ele} at the two electrodes. It thus requires further analyses to explain the linear dependence observed in Figure 3E.

In fact, we found significant blunting of the resistive pulse waveforms via interplay between the resistance and capacitance (Tsutsui et al., 2018). Its effect was examined by fitting the tails with $\Delta I_{ion} \sim \exp(-t/\tau_1)$, where $\tau_1 = RC$ is the time constant of a parallel RC circuit model assumed (Figures 5A and 5B). This expression is valid unless the translocation motions of the nanoparticles exiting the nanopore are much faster than the RC-mediated temporal resolution of the ionic current measurements. The signal pattern analysis revealed a linear relationship between τ_1 and the resistance of the nanopore system, $R = V_b/I_{open}$ (Figure 5C; see also Figure S3), in the whole resistive pulse data including those recorded with not only Ag/AgCl but also Pt electrodes. The relationship as a whole implied the direct relevance of the time-varying R_{ele} to the temporal resolution of nanopore sensors (note that τ_1 scales linearly with R even within the data acquired under a certain salt concentration condition). In this context, it is noticeable that similar trends were reported when varying solution resistance at external regions of nanopores by integrating microchannels on membranes (Kishimoto et al., 2020). The $\tau_1 - R$ dependence thus indicates the major contribution of R_{ele} to alter the out-of-pore resistance contributing to the signal retardation. It is speculated that this gave rise to the linear I_p - I_{open} dependence in Figure 3E.

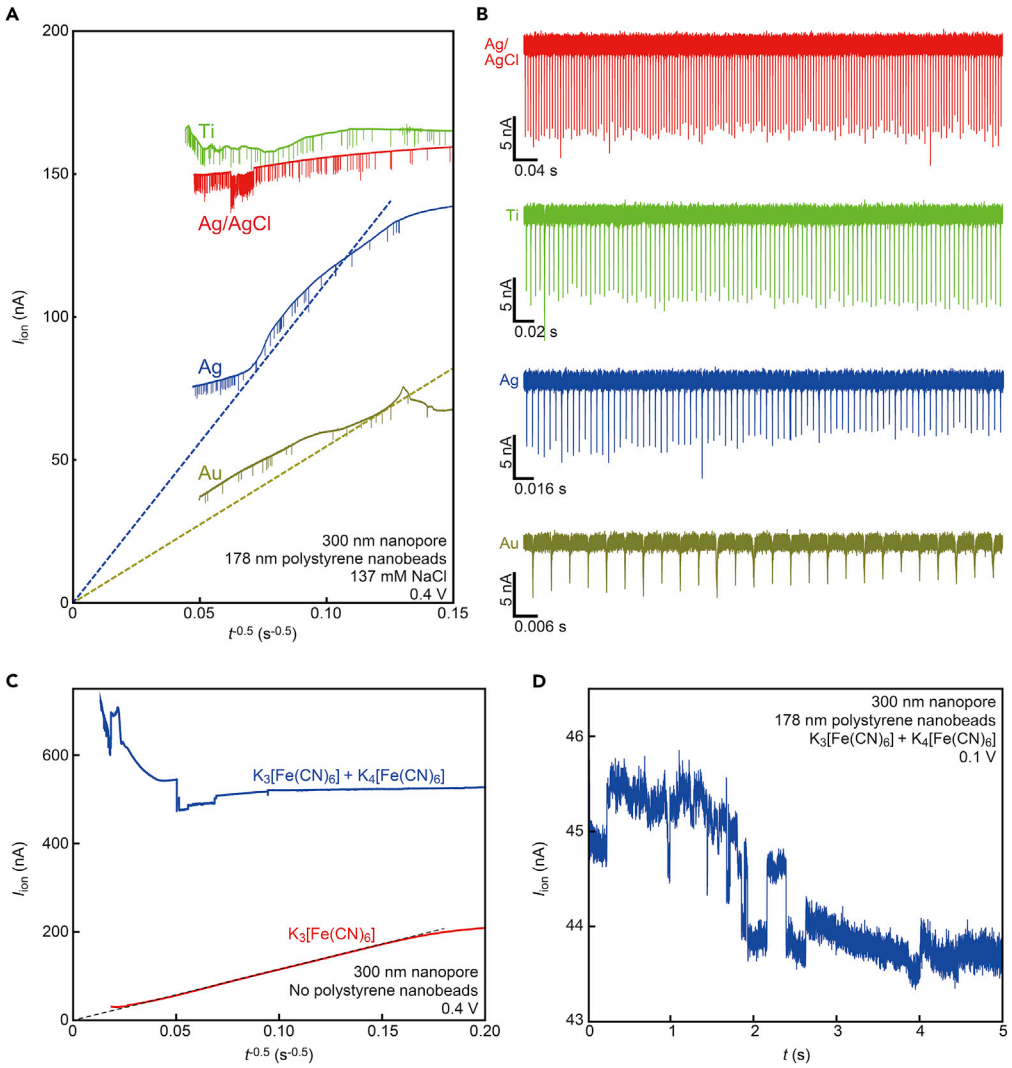

Figure 4. Electrode material and electrolyte dependence of the ionic current characteristics

(A) I_{ion} traces recorded using a 300 nm nanopore under 0.4 V with different metal electrodes: Ag/AgCl (red), Ti (greed), Ag (blue), and Au (dark yellow. Dashed lines are fitting with $I_{ion} \sim t^{-0.5}$.

(B) Resistive pulses obtained for the 178 nm nanobeads within 15 min with various electrodes.

(C) Ionic current traces recorded in aqueous solutions of ferrocyanide using a 300 nm-sized nanopore with platinum electrodes under the transmembrane voltage of 0.4 V. Blue curve is the result in the water solution containing potassium hexacyanoferrate(III) ($K_3[Fe(CN)_6]$) and potassium hexacyanoferrate(II) trihydrate ($K_4[Fe(CN)_6]$) at 0.1 V while red curve is the result in the solution containing only $K_3[Fe(CN)_6]$ at 0.1 M. The ionic current is plotted against $t^{-0.5}$. A stable ionic current was observed with $Fe(CN)_6^{4-}/Fe(CN)_6^{3-}$ due to the redox reaction at the platinum electrodes. In contrast, the absence of reactants with only $K_3[Fe(CN)_6]$ led to diffusion-limited ionic current manifested by the decay in I_{ion} by $t^{-0.5}$ (dashed line is a fit with $I_{ion} \sim t^{-0.5}$).

(D) Resistive pulse measurements of the 178 nm-sized polystyrene beads in the solution of 0.1 M $Fe(CN)_6^{4-}/Fe(CN)_6^{3-}$. No notable features suggestive of particle translocation were observed due presumably to aggregation of the polymeric beads.

In contrast, the curvatures at the left-half of the resistive pulses, which reflects the motions of the nanoparticles at the nanopore entrance, demonstrated a non-trivial manner. While the *RC* retardation is expected to be equally effective to blunt the signals at the onsets and the tails, the time constant τ_2 (assessed by the exponential fits as shown in Figures 6A and 6B) revealed only faint dependence on *R* (Figure 6C). This is in part due to the considerable scattering in the pulse onset line-shapes reflecting the stochastic nature of the

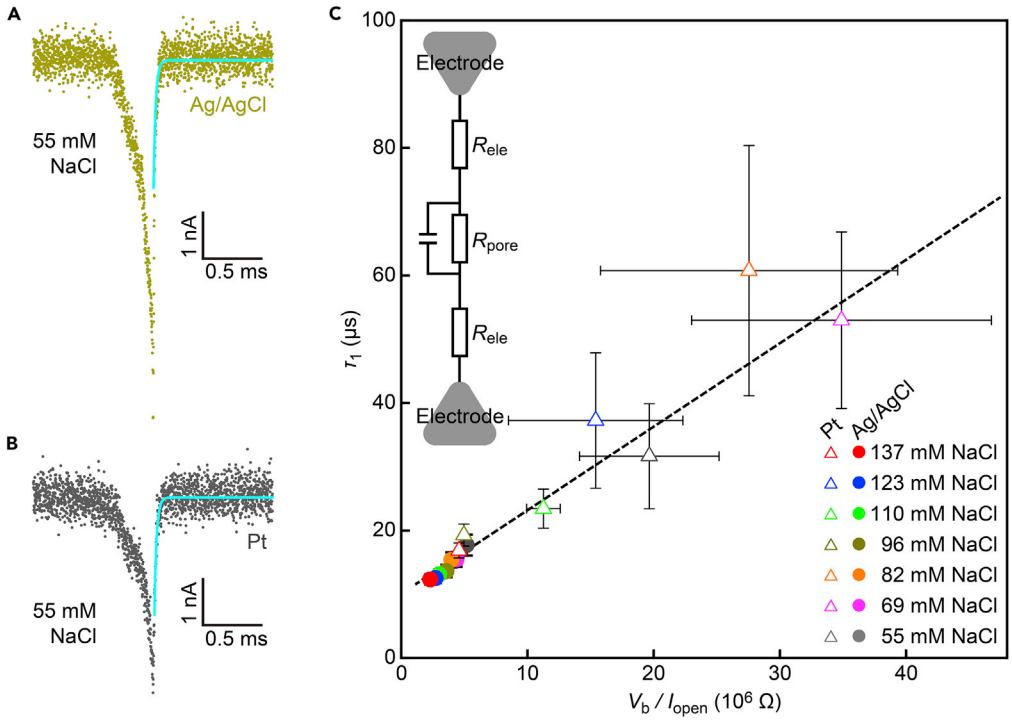

Figure 5. Impedance-limited temporal resolution of the nanopore sensing

(A and B) Typical resistive pulses recorded for the 186 nm-sized nanobeads in 55 mM NaCl solutions with Ag/AgCl (A) and Pt (B) electrodes under V_b of 0.4 V. Sky blue curves are the exponential fits by $I_{ion} \sim -\exp(-t/\tau_1)$ at the signal tails.

(C) τ_1 versus V_b/I_{open} scatter plots. Open triangles and filled circles are the data obtained with Pt and Ag/AgCl electrodes, respectively. Error bars denote the standard deviations. Dashed line is a linear fit to the whole plots. Inset is a refined equivalent circuit explaining the overall dependence of τ_1 on the nanopore resistance.

nanoparticles drawn into the nanopore at random angles (which is not the case after escaping the pore where the inertial effects tend to regulate their translocation motions) (Tsutsui et al., 2019). Another thing is the slow electrophoretic motions of the polymeric beads at the orifice (note that τ_2 is relatively longer than τ_1) allowing the ionic current to catch up with the change in their positions, hence obscuring the trait of the *RC* retardation.

Influence of electrode ion diffusion on particle translocation dynamics

It is also noticeable that τ_2 is electrode-material dependent. In the case of Ag/AgCl, we could find a tendency where τ_2 becomes longer with R when decreasing the salt concentrations (Figure S4). Considering that the resistive pulse onsets mostly represent the translocation dynamics at the orifice rather than the *RC* effects, it can be explained by the slower motions of the polymeric particles under the more effective electroosmotic flow in the diluter electrolyte solution imposing stronger hydrodynamic drag forces to push them back (Figure S5) (Tsutsui et al., 2021; Firnkes et al., 2010; Xu et al., 2021). This is different for the results obtained with Pt, where τ_2, or equivalently the time t_{cap} for the nanobeads to be drawn into the nanopore (Figure 7A), scatters more and tends to become gradually shorter by time within the data collected under a constant salt concentration condition.

Since it is hard to imagine a gradual decrease in the mobility of the polymer spheres or ionic strength of the electrolyte buffer during the resistive pulse measurements, physical mechanisms other than the *RC* coupling should be responsible for the τ_2 (t_{cap}) characteristics. What largely determines the particle motions at the orifice is the balance between the counteracting electrophoretic and hydrodynamic drag forces (Tsutsui et al., 2021; Firnkes et al., 2010; Xu et al., 2021; Stein et al., 2010). As these forces both become stronger with the transmembrane voltage, it gives non-straightforward V_b dependence of the translocation dynamics (Bacri et al., 2011). For the present system, increasing voltage led to a monotonic elongation of

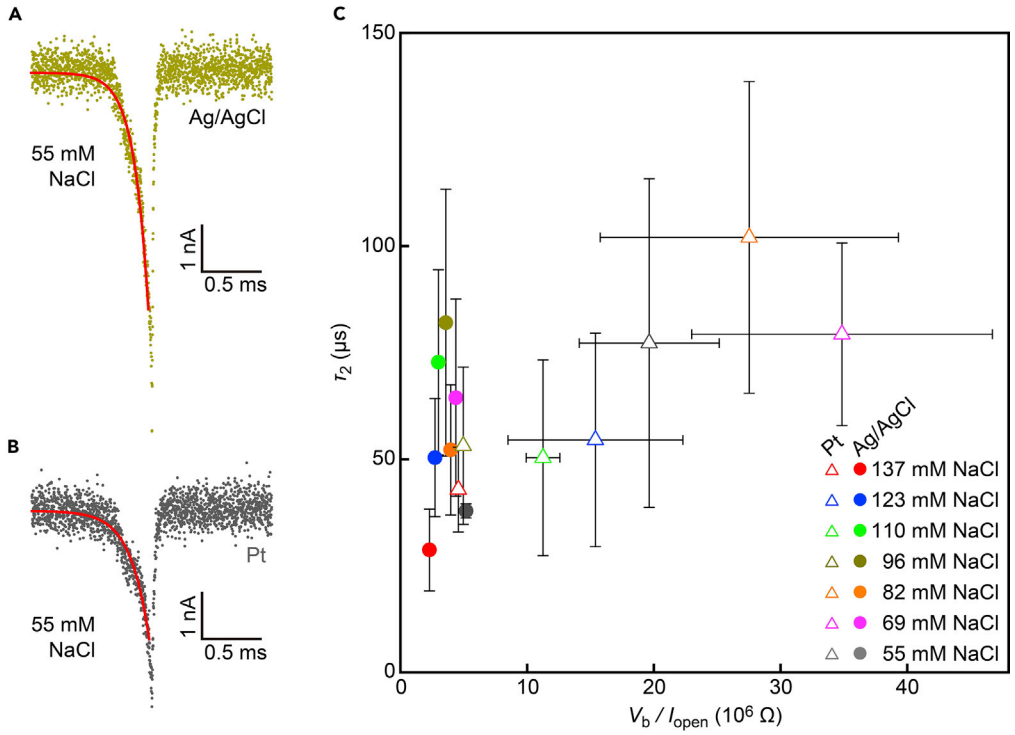

Figure 6. Resistive pulse onset line-shapes

(A and B) Resistive pulses recorded using Ag/AgCl (a) and Pt (b) with fit curves in red by $I_{ion} \sim 1\text{-}\exp(t/\tau_2)$.

(C) τ_2 versus V_b/I_{open} scatter plots shown by open triangles and filled circles for the data obtained with Pt and Ag/AgCl electrodes, respectively. Error bars denote the standard deviations.

t_{cap} manifesting a more rapid increase in the hydrodynamic drag force compared to the electrophoretic counterpart (Figure 7B; see also Figure S6 that explains why t_{cap} increases rapidly at above 0.4 V) (Tsutsui et al., 2021), *i.e.* faster translocation under lower V_b (here, Ag/AgCl was used to avoid the influence of the ion diffusion at the solution/electrode interfaces). Analogous discussion can be made to explain the plots in Figures 6C and 7A. At the beginning of the measurement with Pt electrodes, the impedance at the solution/electrode interfaces was low so that a large portion of V_b was focused at the nanopore. Later, however, the Cottrell diffusion steadily enlarged the interfacial resistance R_{ele} at the electrodes. When it became comparable to R_{pore}, the voltage started to drop largely at the electrodes. As a consequence, the electric potential difference V_{eff} across the nanopore became weaker over time (Figure 7C). Concurrently, it led to shorter t_{cap} by the altered balance between the electrophoretic and hydrodynamic drag forces. In contrast to Pt, the low electrode impedance at the solution-Ag/AgCl interfaces led to $V_{eff} \sim V_b$, and hence relatively long τ_2 due to the electroosmotic flow-derived slow motions of the nanoparticles at the nanopore entrance (with the aforementioned influence of the ionic strength as shown in Figure S4). Although it is not possible to quantify the effect of the interfacial impedance on the translocation dynamics of the nanoparticles due to the uncertainty in the time-evolved resistance distributions between the electrodes and the membrane, the above results elucidate another outcome of the electrode ion diffusion to vary the translocation motions of analytes.

DISCUSSION

The present findings prove the important roles of electrode materials in nanopore sensing. Ag/AgCl is confirmed to be particularly useful to obtain persistent ionic current in a chloride solution for reliable resistive pulse detections of particles and molecules. Unlike the non-polarizable electrodes, electrochemical reactions at the platinum surfaces involve no precipitation/adsorption of reactants, and so induce growing interfacial impedance. This Cottrell diffusion-derived resistance was demonstrated to substantially degrade the temporal resolution of the ionic current measurements as well as to change the translocation dynamics of analytes in a time-varying manner, which would be fatal to discriminate analytes such as viruses

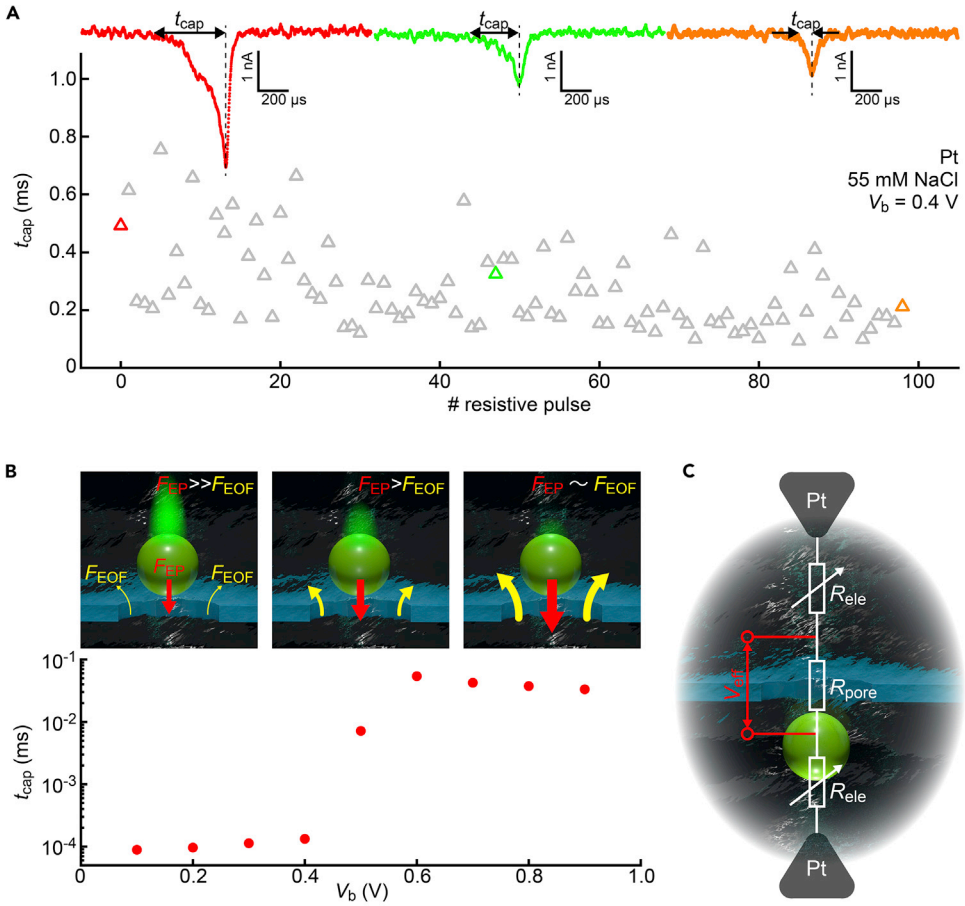

Figure 7. Transmembrane voltage-dependent particle capture dynamics

(A) The width t_{cap} at the first half of the resistive pulses obtained with the Pt-nanopore-Pt setup representing the time required for the particles to be electrophoretically drawn into the nanopore. The resistive pulses correspond to the data displayed as red, green, and orange triangles.

(B) Change in t_{cap} with V_b observed in the resistive pulse measurements using Ag/AgCl electrodes in 55 mM NaCl solution. t_{cap} increases steadily when increasing V_b from 0.1 to 0.6 V signifying a more rapid increase in the electroosmotic forces F_{EOF} than the electrophoretic counterpart (F_{EP}). The sketches depict the relative strength of the electrophoretic and hydrodynamic drag forces on the particles at the nanopore orifice under different transmembrane voltages.

(C) A circuit model explaining the time-varying electric potential difference at the nanopore V_{eff} due to the growing impedance at the solution/Pt interfaces.

(Arima et al., 2020) and proteins (Houghtaling et al., 2018, 2019) by the difference in the ionic signal waveforms. Yet, electrochemistry predicts a way to make such electrodes still useful by employing large electrode surface area with high ionic strength for mitigating the impedance increase to allow resistive pulse sensing for a certain period of time before it becomes comparable to the resistance at a nanopore. Conversely, it also cautions that care should be taken when utilizing microfabricated electrodes that may augment the electrode ion diffusion interference even with Ag/AgCl (Chia et al., 2019).

Limitations of the study

We note that the present work studied the roles of electrode materials for only 300 nm diameter nanopores. Considering that smaller nanopores possess larger R_{pore}, the roles of the Cottrell diffusion may change as the voltage division at R_{ele} would become smaller. On contrary, the choice of electrode materials is predicted to become more important when using micropores where smaller pore resistance gives rise to more pronounced influence of R_{ele} on the ionic current characteristics. Further efforts should be devoted to clarify this point.

STAR★METHODS

Detailed methods are provided in the online version of this paper and include the following:

- KEY RESOURCES TABLE
- RESOURCE AVAILABILITY
  - Lead contact
  - Materials availability
  - Data and code availability
- METHOD DETAILS
  - Fabrication of micro- and nanopores
  - Resistive pulse measurements
  - Data analyses
  - Finite element simulations

SUPPLEMENTAL INFORMATION

Supplemental information can be found online at https://doi.org/10.1016/j.isci.2022.105073.

ACKNOWLEDGMENTS

A part of this work was supported by the Japan Society for the Promotion of Science (JSPS) KAKENHI Grant Number 22H01926.

AUTHOR CONTRIBUTIONS

Conceptualization, M. Tsutsui and M. Taniguchi; Methodology, I.W.L., S.K., and M. Tsutsui; Investigation, I.W.L., S.K., and M. Tsutsui; Writing- Original Draft, M. Tsutsui; Writing – Review & Editing, M. Tsutsui; Funding Acquisition, M. Tsutsui; Resources, M. Tsutsui.

DECLARATION OF INTERESTS

The authors declare no competing interests.

Received: July 7, 2022
Revised: August 6, 2022
Accepted: August 30, 2022
Published: October 21, 2022

SUPPORTING CITATIONS

The following references appear in the Supplemental information: Ermann et al., 2018; Yukimoto et al., 2013.

REFERENCES

Arima, A., Tsutsui, M., Yoshida, T., Tatematsu, K., Yamazaki, T., Yokota, K., Kuroda, S., Washio, T., Baba, Y., and Kawai, T. (2020). Digital pathology platform for respiratory tract infection diagnosis via multiplex single-particle detections. ACS Sens. *5*, 3398–3403.

Bacri, L., Oukhaled, A.G., Schiedt, B., Patriarche, G., Bourhis, E., Gierak, J., Pelta, J., and Auvray, L. (2011). Dynamics of colloids in single solid-state nanopores. J. Phys. Chem. B *115*, 2890–2898.

Baehre, D., Ernst, A., Weißhaar, K., Natter, H., Stolpe, M., and Busch, R. (2016). Electrochemical dissolution behavior of titanium and titanium-based alloys in different electrolytes. Procedia CIRP *42*, 137–142.

Chia, C., Jeffrey, S.S., and Howe, R.T. (2019). Anomalous hysteresis and current fluctuations in cyclic voltammograms at microelectrodes due to Ag leaching from Ag/AgCl electrodes. Electrochem. Commun. *105*, 106499.

Ermann, N., Hanikel, N., Wang, V., Chen, K., Weckman, N.E., and Keyser, U.F. (2018). Promoting single-file DNA translocations through nanopores using electro-osmotic flow. J. Chem. Phys. *149*, 163311.

Firnkes, M., Pedone, D., Knezevic, J., Döblinger, M., and Rant, U. (2010). Electrically facilitated translocations of proteins through silicon nitride nanopores: conjoint and competitive action of diffusion, electrophoresis, and electroosmosis. Nano Lett. *10*, 2162–2167.

Fried, J.P., Swett, J.L., Nadappuram, B.P., Mol, J.A., Edel, J.B., Ivanov, A.P., and Yates, J.R. (2021). In situ solid-state nanopore fabrication. Chem. Soc. Rev. *50*, 4974–4992.

Gao, R., Lin, Y., Ying, Y.L., Hu, Y.X., Xu, S.W., Ruan, L.Q., Yu, R.J., Li, Y.J., Li, H.W., Cui, L.F., and Long, Y.T. (2019). Wireless nanopore electrodes for analysis of single entities. Nat. Protoc. *14*, 2015–2035.

Garaj, S., Hubbard, W., Reina, A., Kong, J., Branton, D., and Golovchenko, J.A. (2010). Graphene as a subnanometre trans-electrode membrane. Nature *467*, 190–193.

He, Y., Tsutsui, M., Zhou, Y., and Miao, X.-S. (2021). Solid-state nanopore systems: from materials to applications. NPG Asia Mater. *13*, 48.

Henriquez, R.R., Ito, T., Sun, L., and Crooks, R.M. (2004). The resurgence of Coulter counting for analyzing nanoscale objects. Analyst *129*, 478–482.

Holz, M., Heil, S.R., and Sacco, A. (2000). Temperature-dependent self-diffusion coefficients of water and six selected molecular liquids for calibration in accurate ^{1}H NMRPFG measurements. Phys. Chem. Chem. Phys. *2*, 4740–4742.

Houghtaling, J., List, J., and Mayer, M. (2018). Nanopore-based, rapid characterization of individual amyloid particles in solution: concepts, challenges and prospects. Small *14*, 1802412.

Houghtaling, J., Ying, C., Eggenberger, O.M., Fennouri, A., Nandivada, S., Acharjee, M., Li, J., Hall, A.R., and Mayer, M. (2019). Estimation of shape, volume, and dipole moment of individual proteins freely translocating a synthetic nanopore. ACS Nano *13*, 5231–5242.

Hu, Z., Huo, M., Ying, Y., and Long, Y. (2020). Biological nanopore approach for single-molecule protein sequencing. Angew. Chem. *133*, 14862–14873.

Jaksic, M., Johansen, B., and Tunold, R. (1993). Electrochemical behaviour of platinum in alkaline and acidic solutions of heavy and regular water. Int. J. Hydrogen Energy *18*, 817–837.

Kishimoto, S., Murayama, S., Tsutsui, M., and Taniguchi, M. (2020). Crucial role of out-of-pore resistance on temporal response of ionic current in nanopore sensors. ACS Sens. *5*, 1597–1603.

Kowalczyk, S.W., Grosberg, A.Y., Rabin, Y., and Dekker, C. (2011). Modeling the conductance and DNA blockade of solid-state nanopores. Nanotechnology *22*, 315101.

Lee, G.-Y., Park, J.-H., Chang, Y.W., Cho, S., Kang, M.-J., and Pyun, J.-C. (2018). Chronoamperometry-based redox cycling for application to immunoassays. ACS Sens. *3*, 106–112.

Lee, S.H., and Rasaiah, J.C. (2011). Proton transfer and the mobilities of the H^{+} and OH^{-} ions from studies of a dissociating model for water. J. Chem. Phys. *135*, 124505.

Liao, C., Antaw, F., Wuethrich, A., Anderson, W., and Trau, M. (2020). Configurable miniaturized 3D pores for robust single-nanoparticle analysis. Small Struct. *1*, 2070006.

Luo, J., Sam, A., Hu, B., DeBruler, C., Wei, X., Wang, W., and Liu, T.L. (2017). Unraveling pH dependent cycling stability of ferricyanide/ferrocyanide in redox flow batteries. Nano Energy *42*, 215–221.

Messerschmitt, F., Kubicek, M., Schweiger, S., and Rupp, J.L. (2014). Memristor kinetics and diffusion characteristics for mixed anionic-electronic $SrTiO_{3-\delta}$ bits: the memristor-based Cottrell analysis connecting material to device performance. Adv. Funct. Mater. *24*, 7448–7460.

Mojtabavi, M., Tsai, W.-Y., Vahid-Mohammadi, A., Zhang, T., Gogotsi, Y., Balke, N., and Wanunu, M. (2022). Ionically active MXene nanopore actuators. Small *18*, 2105857.

Plesa, C., Kowalczyk, S.W., Zinsmeester, R., Grosberg, A.Y., Rabin, Y., and Dekker, C. (2013). Fast translocation of proteins through solid-state nanopores. Nano Lett. *13*, 658–663.

Plesa, C., Ruitenberg, J.W., Witteveen, M.J., and Dekker, C. (2015). Detection of individual proteins bound along DNA using solid-state nanopores. Nano Lett. *15*, 3153–3158.

Pletcher, D., Greef, R., Peat, R., Peter, L.M., and Robinson, J. (2011). Instrumental Methods in Electrochemistry (Woodhead Publishing Limited).

Stein, D., Deurvorst, Z., van der Heyden, F.H.J., Koopmans, W.J.A., Gabel, A., and Dekker, C. (2010). Electrokinetic concentration of DNA polymers in nanofluidic channels. Nano Lett. *10*, 765–772.

Sun, T., and Morgan, H. (2010). Single-cell microfluidic impedance cytometry: a review. Microfluid. Nanofluid. *8*, 423–443.

Tsutsui, M., Yokota, K., Arima, A., Tonomura, W., Taniguchi, M., Washio, T., and Kawai, T. (2018). Temporal resolution of ionic current blockade in solid-state nanopores. ACS Appl. Mater. Interfaces *10*, 34751–34757.

Tsutsui, M., Yokota, K., Arima, A., He, Y., and Kawai, T. (2019). Solid-state nanopore time-of-flight mass spectrometer. ACS Sens. *4*, 2974–2979.

Tsutsui, M., Ryuzaki, S., Yokota, K., He, Y., Washio, T., Tamada, K., and Kawai, T. (2021). Field effect control of translocation dynamics in surround-gate nanopores. Commun. Mater. *2*, 29.

van der Niet, M.J., Garcia-Araez, N., Hernández, J., Feliu, J.M., and Koper, M.T. (2013). Water dissociation on well-defined platinum surfaces: the electrochemical perspective. Catal. Today *202*, 105–113.

van Dorp, S., Keyser, U.F., Dekker, N.H., Dekker, C., and Lemay, S.G. (2009). Origin of the electrophoretic force on DNA in solid-state nanopores. Nat. Phys. *5*, 347–351.

Wang, D., Wang, Y., Li, H., Han, Y., Hu, P., Ma, K., Sheves, M., and Jin, Y. (2022). Photoactivated bacteriorhodopsin/SiN_x nanopore-based biological nanofluidic generator with single-protein sensitivity. ACS Nano *16*, 1589–1599.

Xu, C., Liu, Y., Xiong, T., Wu, F., Yu, P., Wang, J., and Mao, L. (2021). Dynamic behavior of charged particles at the nanopipette orifice. ACS Sens. *6*, 2330–2338.

Xue, L., Yamazaki, H., Ren, R., Wanunu, M., Ivanov, A.P., and Edel, J.B. (2020). Solid-state nanopore sensors. Nat. Rev. Mater. *5*, 931–951.

Yukimoto, N., Tsutsui, M., He, Y., Shintaku, H., Tanaka, S., Kawano, S., Kawai, T., and Taniguchi, M. (2013). Tracking single-particle dynamics via combined optical and electrical sensing. Sci. Rep. *3*, 1855.

Zhang, Y., Zhang, B., and White, H.S. (2006). Electrochemistry of nanopore electrodes in low ionic strength solutions. J. Phys. Chem. B *110*, 1768–1774.

STAR★METHODS

KEY RESOURCES TABLE

REAGENT or RESOURCE	SOURCE	IDENTIFIER
Chemicals, peptides, and recombinant proteins		
Phosphate buffered saline	Nippon Gene	Cat#: 314-90185
Polystyrene beads	Polysciences	Cat#: 08216-15
Potassium ferricyanide K3Fe(CN)6	Fujifilm Wako Chemicals	Cat#: 167-03722
Potassium ferricyanide K4Fe(CN)6	Fujifilm Wako Chemicals	Cat#: 161-03742

RESOURCE AVAILABILITY

Lead contact

Further information and requests for resources should be directed to and will be fulfilled by the lead contact, Makusu Tsutsui (tsutsui@sanken.osaka-u.ac.jp).

Materials availability

This study did not generate new unique reagents.

Data and code availability

- All data reported in this paper will be shared by the lead contact upon request.
- This paper does not report original code.
- Any additional information required to reanalyze the data reported in this paper is available from the lead contact upon request.

METHOD DETAILS

Fabrication of micro- and nanopores

A 4-inch silicon wafer both sides of the surfaces covered with the low-pressure chemical vapor deposition-grown SiN_x layers of 50 nm thickness was purchased from Electronics & Materials Co. and used as substrates after dicing into 30 mm × 30 mm pieces with a dicer. SiN_x at one side of the substrate was partially removed by reactive ion etching through a metal mask, which created an approximately 1 mm square area of Si. The Si surface was then exposed to KOH aq. and heated to 80°C for deep wet etching. This formed a trench with a 40 nm-thick SiN_x membrane at the bottom (due to thinning of the SiN_x by about 10 nm during the wet etching). On the SiN_x membrane, an electron beam resist ZEP520A (Zeon) was spin-coated. After baking at 180°C, a circle of diameter 300 nm was delineated by an electron beam lithography. Developing the pattern, the substrate was treated with the reactive ion etching to open a nanopore, where the residual resist layer served as a mask. Finally, the nanopore chip was immersed in *N,N* Dimethylformamide overnight to dissolve the resist followed by rinsing with ethanol and acetone.

Resistive pulse measurements

Polymer blocks were prepared by curing PDMS precursor (Sylgard184, Dow) and baking at 80°C for 5 h. The blocks were adhered on both sides of the nanopore chip by activating the surfaces with oxygen plasma. Three holes were punched in the blocks that served as inlet and outlet of sample solution as well as a place to put the electrode, either a Ag/AgCl or Pt rod of diameter 0.8 mm, for the ionic current measurements. After filling the pore with dilute suspension of nominally 200 nm-sized carboxylated polystyrene nanobeads (Polysciences) in diluted phosphate buffered saline, the voltage V_b was applied to one of the electrodes and the output ionic current was measured through the other electrode at 1 MHz using a custom-designed current amplifier and a digitizer (NI-5922, NI).

Data analyses

Resistive pulses were extracted from the raw ionic current curves by first offsetting the open pore current to zero. This was implemented by subtracting the linearly-fit components in every 0.5 s region. The pulse

signals were then identified by searching local minima of the ionic current using a threshold level of −1 nA. Subsequently, the ionic current data of 5 milliseconds before and after each minimal point were saved. The resistive pulses obtained in this way were then fit by exponential functions to deduce τ_1 and τ_2. All the computational tasks were performed by codes written in Python.

Finite element simulations

Ionic blockade current and electroosmotic flow velocity in a nanopore were simulated with coupled Poisson-Nernst-Planck and Navier-Stokes equations using AC/DC, Chemical Reaction Engineering, and Computational Fluid Dynamics (CFD) modules in COMSOL. We defined a 25 μm diameter and 40 nm thick SiN_x disk with a hole of 150 nm radius at the center in a cylindrical coordinate system. The nanopore was filled with NaCl solution of dynamic viscosity of $\eta = 10^{-3}$ Pa s. Surface charge density of polystyrene beads and nanopore wall surface was set according to the zeta potential measured using a zeta-sizer (Malvern Panalytical). The permittivity of SiN_x and water was assumed to be the same as that of the bulk.